Romanian Reports in Physics, Vol. 66, No. 3, P. 693–703, 2014

PAN/PDLLA FIBERS WITH MAGNETIC MINERAL NANOPARTICLES INSERTION FOR CONTROLLED RELEASE OF DRUGS

S. VULPE[1,2], GABRIELA NEGROIU[2], CLAUDIA NASTASE[1], F. NASTASE[1], T.L. MITRAN[3], C. BERBECARU[3], C. NECULA[4], ADELA MARIN[5]

[1] University of Bucharest, Polymer Science Group, P.O. Box MG–40 Magurele, 077125, Bucharest, Romania, E-mail: vulpesilviu@psg.unibuc.ro
[2] Institute of Biochemistry of the Romanian Academy, Splaiul Independentei 296, 060031, P.O. Box 17, Bucharest, Romania
[3] University of Bucharest, Electricity&Magnetism, Solid-State Physics, Biophysics Dept., P.O. Box MG–11 Magurele, 077125, Bucharest, Romania
[4] University of Bucharest, Structure of Matter, Physics of the Earth, Atmospheric Physics, and Astrophysics Dept., P.O. Box MG–11 Magurele, 077125,Bucharest, Romania
[5] University of Bucharest, Faculty of Biology, Department of Anatomy, Animal Physiology and Biophysics, Splaiul Independentei 91-95, 050095, Bucharest, Romania

Received March 21, 2013

Abstract. We report the design and obtaining method of polyacrylonitrile (PAN)/Poly(DL lactide) acid fibers with nano magnetic particles of Fe_3O_4. The results of morphological characterization show that nano-magnetite particles are well distributed throughout the composite. The magnetic investigations of the prepared nanocomposites show that they could become a potential candidate for a kind of specific biomedical application due to their strong magnetization.

Key words: nanocomposites, magnetic nanoparticles, electrospinning, controlled release.

1. INTRODUCTION

Targeted delivery and controlled release of drugs represent domains of great interest. Structures for transport and controlled release of drugs with high affinity for certain organs, tissues and cells, were introduced in 1906, when Paul Ehrlich postulated for the first time the concept of "magic bullet" [1].

Transportation systems and controlled release of drugs include: liposomes [2–4], polymeric micelles [5–7], artificial DNA nanostructures [8–10], nanoparticles [11–14] and magnetic nanoparticles (MNPs) [15–18]. Out of these, in recent years, magnetic nanoparticles have drawn increased attention of researchers.

MNPs have controllable sizes ranging from few nanometers up to tens of nanometers, which place them at dimensions that are smaller or comparable to those of a living cell, a virus, a protein or a gene. This means that they can approach to a biological entity of interest and can be manipulated by an external magnetic field gradient (they obey Coulomb's law) [19]. This propriety opens up many applications involving the transport and/or immobilization of MNPs. MNPs can be chemically and structurally manipulated for creating numerous variants able to efficiently deliver anti-cancer drugs or a group of radionuclides to an organ containing a specific tumor [20]. MNPs can be constructed in such a way as to resonantly respond to a time-varying magnetic field, with advantageous results related to the transfer of energy from the exciting field to the nanoparticle.

The major requirements for MNPs to efficiently act in biological systems are: biocompatibility and the capacity to be directed through the bloodstream. Biocompatibility has been achieved by coating MNPs with various well-tolerated polymeric (natural or synthetic) structures, whereas the directed flow of MNPs through the bloodstream still represents a challenge. A possible solution to this problem could be the increase of Fe_3O_4 particles magnetization. This would ensure that MNPs are not absorbed by the reticuloendotelial system and overcome the forces of mutual attraction after turning of the magnetic field.

Such a "magnetic nanosystem" which meets the above presented requirements can be achieved by using an electrospining process with changed collector geometry (Figure 1).

We report here the design and obtaining method of polyacrylonitrile (PAN)/Poly(DL lactide) acid (PDLLA) fibers with nano magnetic Fe_3O_4 particles. The PAN/PDLLA–Fe_3O_4 nanofibrous composites are expected to produce functional structures with further applicability in the field of drug delivery systems.

2. EXPERIMENTAL

2.1. MATERIALS

Polyacrylonitrile (PAN, M_W = 150,000 g/mol, Sigma-Aldrich Chemical Company, Inc.) have excellent characteristics, which include thermal stability and tolerance to most solvents, atmosphere, bacteria and photo irradiation. Also, PAN fibers have been successfully reported as drug carriers [21].

Poly(DL lactide) (PDLLA, average M_w = 75,000–120,000 g/mol, Sigma-Aldrich Chemical Company, Inc.) – the choice of PDLLA is based on its biocompatibility, biostability and extended use in the biomedical field, particularly in strengthening of some biopolymer or in bone–defect restoration.

Fe_3O_4 magnetic nanoparticles (M = 231,54 g/mol, 98 %, 20–30 nm, specific surface area > 60 m^2/g, black powder, Alfa Aesar) are so far the most commonly

used magnetic carriers for a variety of biomedical applications since their biocompatibility has already been proven [22]. The solvent, N, N-Dimethylformamide (DMF), purity 99.9% was purchased from Merck.

2.2. EXPERIMENTAL CONDITIONS

The solutions for electrospinning were prepared as follows: 0.1 g PAN, 0.1 g PDLLA and an appropriate amount of Fe_3O_4 particles (range from 0.001 to 0.007 g) were dissolved in 2 ml DMF under constant magnetic stirring for about 3 h in order to obtain a homogeneous solution.

All solutions were directly electrospun under the same conditions using typical electrospinning setup (Fig. 1). Each solution was briefly drawn into a glass syringe, and then was electrospun using 15–18 kV high voltage power supply attached to the needle at ambient temperature. The high voltage stretches the solution droplet into a Taylor cone and an electrified jet is formed. The jet is continuously elongated by electrostatic charge repulsion and solvent evaporation, creating a mat of electrospun fibers on the grounded collector surface. The distance between the syringe tip and the collector was ~ 6 cm. The cylindrical rotor was set at 600 rotations per minute.

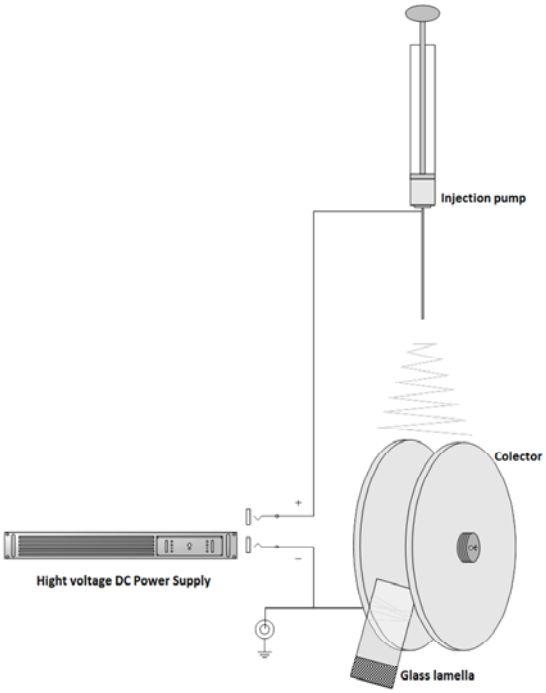

Fig. 1 – Experimental setup for the electrospinning process used to prepare the polymeric magnetic nanofibrous composites.

2.3. INVESTIGATION METHODS

The morphological characterizations of samples were performed using Scanning Electron Microscopy (SEM) and Atomic Force Microscopy (AFM). Images of SEM were obtained using a SEM – TESCAN VEGA XM system operated at 30 kV accelerating voltage and 118 μA emission current. AFM morphology measurements were performed with an atomic force microscope NT–MDT model NTEGRA Aura operating in semi–contact mode. The Fourier Transform-Infrared spectrometry (FT–IR) was performed with Jasco FT–IR–6200 spectrometer. Vibration sample magnetometery (VSM) measurements were performed with MicroMag AGM/VSM model 2900/3900 with low (liquid nitrogen) and high temperature accessories for the VSM head (Princeton Measurements).

Hysteresis loops of the selected samples were measured using Princeton Measurements Corporation Vibrating Sample Magnetometer 3900 in a maximum field of 1T. Hysteresis parameters (saturation magnetization, M_s, remanent magnetization, M_{rs}, and coercive force, H_c were determined after the correction made for para– or diamagnetic contributions identified from the slope at high fields. First–order reversal curve (FORC) measurements were conducted using the same PMC VSM 3900 magnetometer. To construct a FORC diagram, 111 first–order reversal curves were measured using a saturating field of 1T. The FORC data processing was performed using FORCinel software developed by Harrison and Feinberg [23]. The calculation of first–order reversal curve (FORC) diagrams use locally weighted regression smoothing and can perform an optimum smoothing factor calculation. IRM time dependent measurement was performed using the same VSM magnetometer.

3. RESULTS AND DISCUSSION

3.1. SCANNING ELECTRON MICROSCOPY

In the SEM images fibrillar structures derived from polylactic acid containing Fe_3O_4 nanoparticles could be observed. They have diameters between 1.2–1.5 μm (Fig. 2 a,b), 1.0–1.2 μm (Fig. 2 c,d) and 0.9–1.2 μm (Fig. 2 e,f). One can notice a decrease in fibers diameter with decreasing the concentration of nanoparticles. Also, the sizes of nanofibres have been influenced by the heterogeneity of Fe_3O_4 particles, present in all the samples.

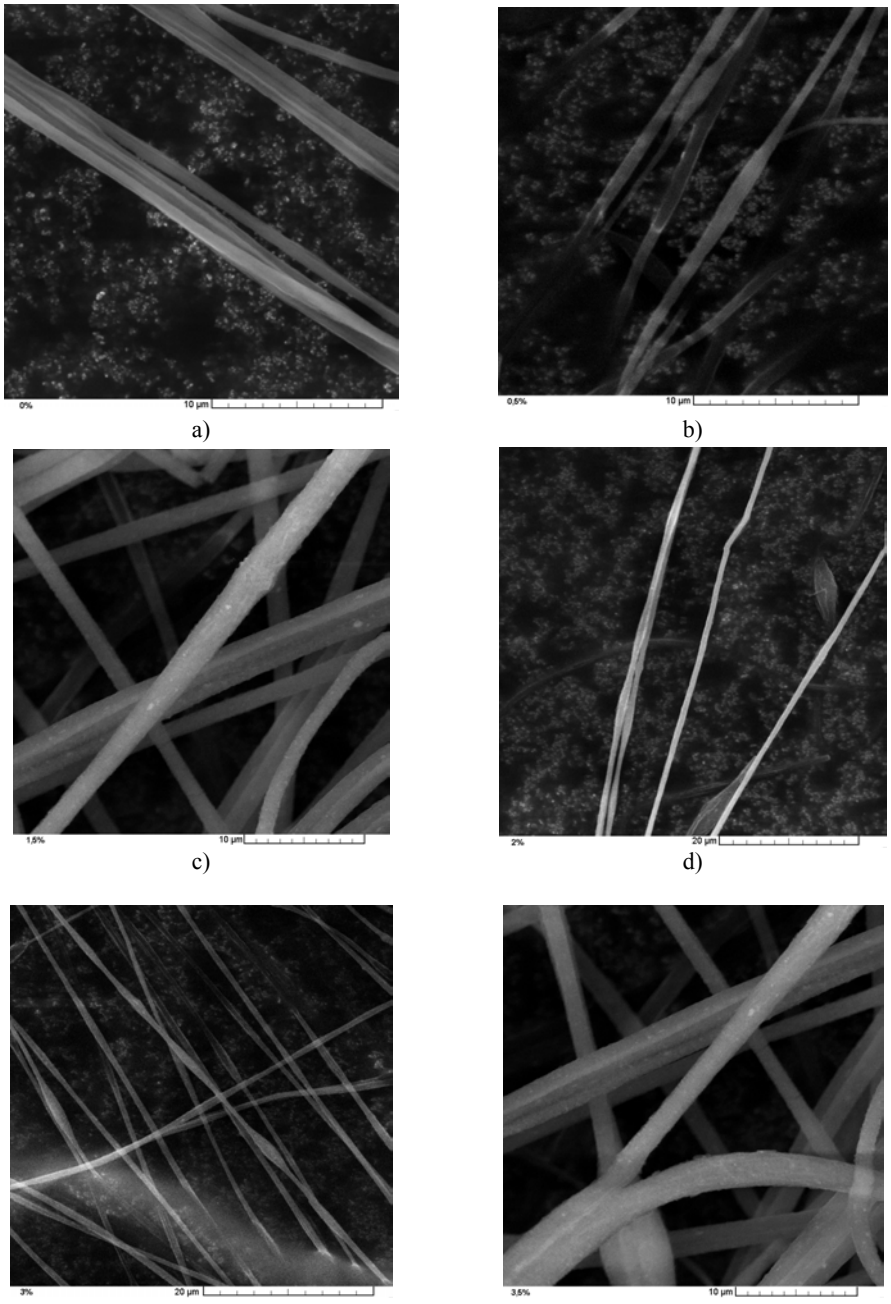

Fig. 2 – Micrographs of PAN/PDLLA– Fe_3O_4 nanocomposite fibers with different Fe_3O_4 nanoparticles weight % content: a) 0%, b) 0,5%, c) 1,5%, d) 2,0%, e) 3,0%, f) 3,5%.

3.2. ATOMIC FORCE MICROSCOPY

Atomic force microscopy was used to obtain topographic images of PAN/PDLLA fiber containing embedded Fe_3O_4 nanoparticles, with diameters ranging from 500 to 900 nm (Fig. 3). Using AFM it can be seen the flashing mode of nanoparticles position, relative to the polymer matrix. The nanoparticles are completely covered by the polymer and their position along the fiber could not be determined.

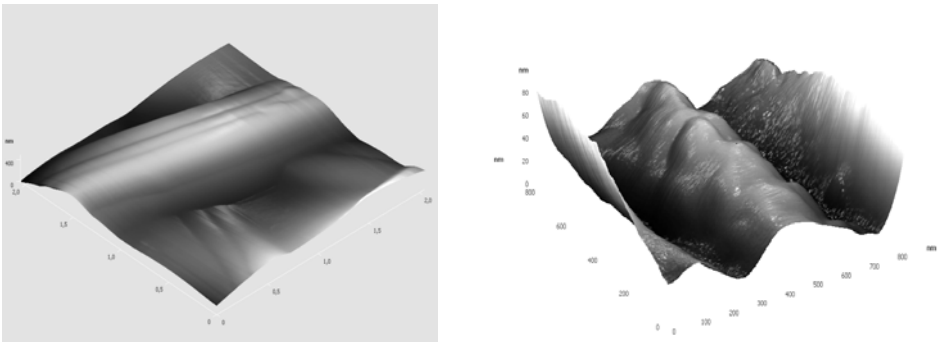

a) b)

Fig. 3 – AFM images of PAN/PDLLA/ Fe_3O_4 nanocomposite fibers: a) fibers without magnetical nanoparticles; b) PAN/PDLLA fibers containing 3.5 weight % Fe_3O_4 nanoparticles.

3.3. FT-IR SPECTROSCOPY

Fourier transform infrared spectroscopy (FT–IR) was used for all obtained samples, due to the distinct absorption modes of amorphous and crystalline components in specific bands. Figure 4 shows the IR spectra in the range 1300–500 cm^{-1} of PAN/PDLLA fibers at different concentrations of magnetite and spectrum of pure magnetite.

The lines of interest are those of the inorganic elements. Their presence and especially their changes in intensity provide information about the behavior of magnetite particles. In the FT–IR spectra there are two specific vibrational lines of Fe–O bonds in Fe_3O_4 located at 550 cm^{-1} and 625 cm^{-1} respectively. The lines corresponding to these types of vibrations do not change their intensities with the increase of magnetite concentration. This figure suggests that the structure of the magnetic particles remains unchanged. Increasing the concentration of magnetite induces configuration changes, reflecting close packing of segments around the main axis. This changes further lead to improved mechanical properties in the deformation behavior and visco-elasticity.

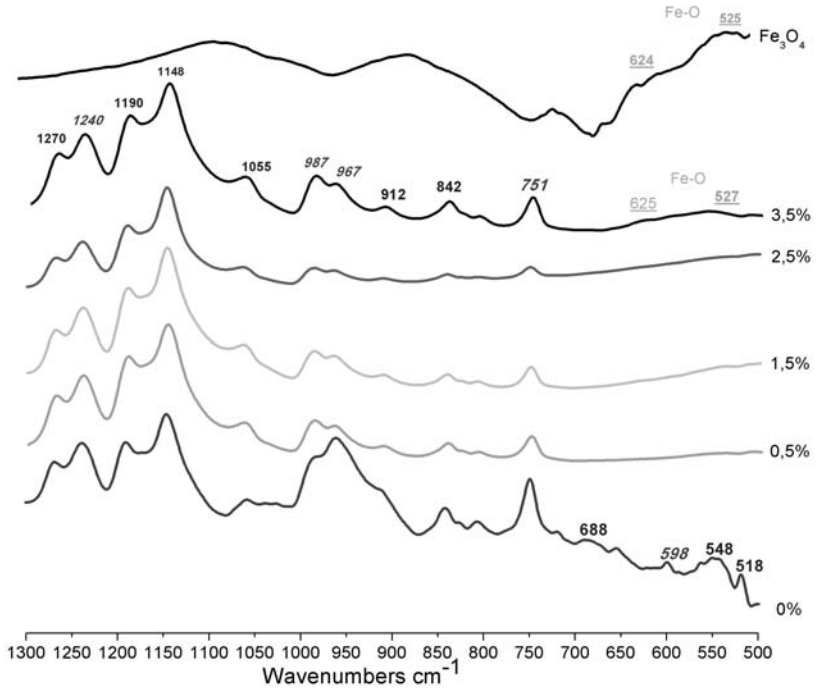

Fig. 4 – FT–IR spectra for PAN/PDLLA composites with different concentration of Fe_3O_4.

Major contributions of peaks in the FTIR spectra are presented in Fig. 4 (italic font for PAN, normal font for PDLLA, and underlined fonts for Fe_3O_4) and Table 1, which were ascribed for bond stretching, between iron and oxide ions of Fe_3O_4. The Fe_3O_4 magnetic nanoparticles are embedded in polymer matrix and do not introduce structural modifications. This is in concordance with magnetic measurements: magnetization increases with iron oxide concentration, and Fe_3O_4 nanoparticles do not interact because they are well dispersed and embedded.

Table 1

FT–IR data: peak band assignments for PAN/PDLLA–Fe_3O_4 nanocomposite fibers

PDLLA (cm^{-1})	PAN (cm^{-1})	Fe_3O_4 (cm^{-1})	Assignment	References
1270			δCH+νCOC	[27-30]
	1240		δCH_2	[24-26]
1190			$\nu_{as}COC$	[27-30]
1148			$r_{as}CH_3$	[27-30]
1055			$\nu C\text{-}CH_3$	[27-30]
	987		δCH	[24-26]
	967		δCH	[24-26]

Table 1 (continued)

912			rCH$_3$+νCC	[27-30]
842			νC-COO	[27-30]
	751		δCH	[24-26]
688			γC=O	[27-30]
		625	Fe-O	[31, 32]
	598		C–C	[24-26]
		550	Fe-O	[31, 32]
548			C–C	[27-30]
518			δ_1C-CH$_3$+δCCO	[27-30]

3.4. VIBRATION SAMPLE MAGNETOMETERY

The ratio of saturation magnetization remanence to saturation magnetization, M_{rs}/M_s, *versus* the ratio of remanence coercivity force to ordinary coercivity force, H_{cr}/H_c, for various concentrations and initial Fe_3O_4 powder (20–40 nm) are shown in Fig. 5.

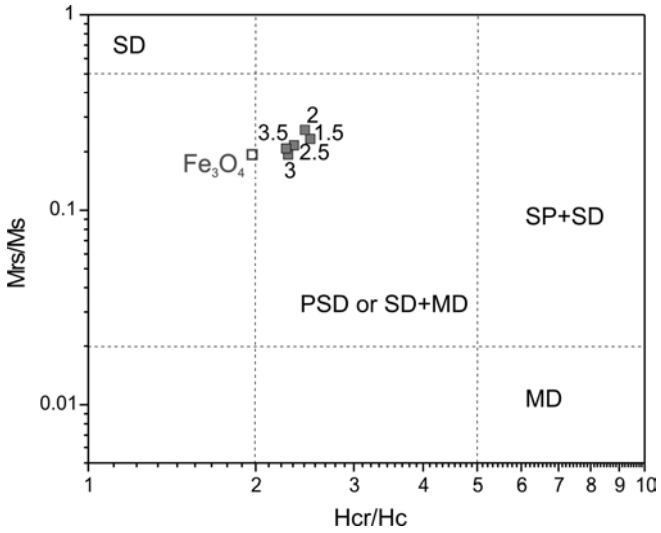

Fig. 5 – Day plot: The ration of saturation remanence to saturation magnetization, M_{rs}/M_s, *versus* ratio of remanence coercivity force to ordinary coercivity force, H_{cr}/H_c.

Limits for SD (single domain), PSD (pseudo-single domain) and MD (multidomain) regions are presented after Dunlop [33]. The experimental data for different concentrations are well grouped into a small region not far from the initial Fe_3O_4 powder. This difference, also visible in the hysteresis curves from Fig. 6, is probably explained by the strong particles interaction in the Fe_3O_4 powder sample.

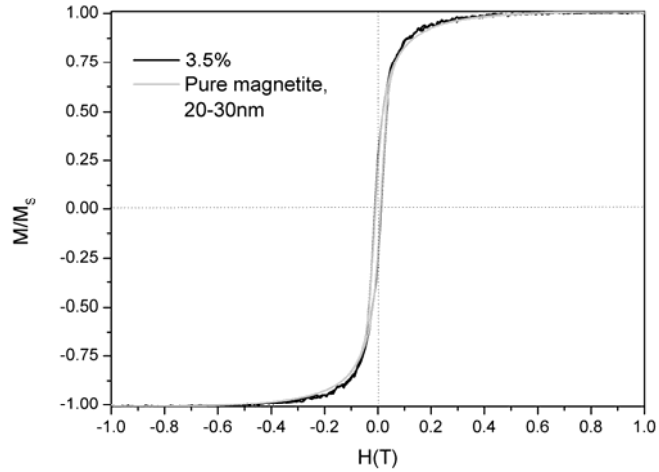

Fig. 6 – Comparison of hysteresis loops for pure magnetite and PAN/PDLLA fibers containing 3.5 % weight Fe_3O_4 nanoparticles.

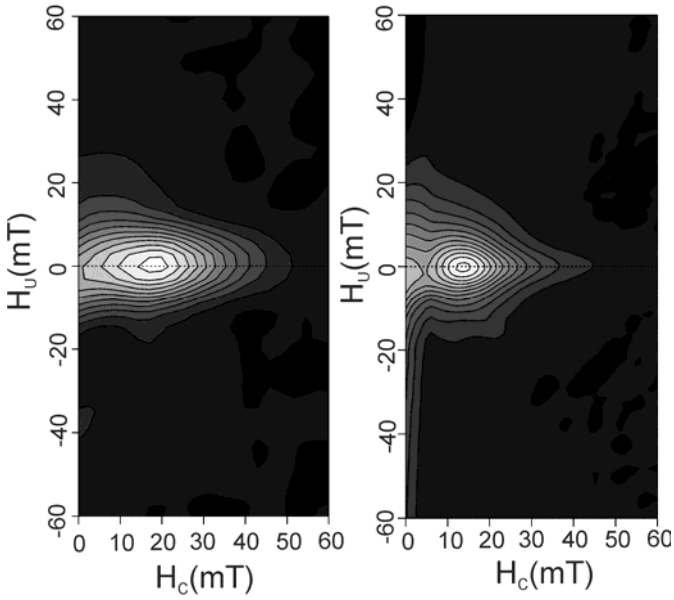

Fig. 7 – First-order reversal curve (FORC) diagrams for PAN/PDLLA fibers containing 3.5 % weight Fe_3O_4 nanoparticles (left) and for pure magnetite (right).

First-order reversal curve (FORC) diagrams represent a powerful tool which can provide detailed information about magnetostatic interactions, domain state and composition [34]. The pure magnetite sample shows a FORC distribution with two peaks (Fig. 7). The first small peak, highlighted by the open contour located

just near the origin of the FORC diagram (H_c well below 10 mT) indicate that the distribution have been shifted to lower coercivities by thermal relaxation effects. This represents the characteristic behavior of superparamagnetic particles [35]. The secondary, very high peak concentrated along the H_c axis (at $H_u = 0$) highlighted by the closed contours represent the signature of non-interacting SD particles. The small spreading along the H_u axis indicates that this sample is affected by a weak local interaction field. This is in concordance with the grain size distribution of the pure magnetite used here; the diameters ranges between 20 and 30 nm and the SP/SSD (superparamagnetic/stable single domain) boundary is approximately at 20 nm [36].

The 3.5% sample shows only a single peak FORC distribution but it is very similar to the pure magnetite one, which has similar in hysteresis curves (Fig. 7). Closed concentric contours surrounding the peak suggest that only SD particles are present in this sample. As for the pure magnetite sample, this one shows a similar spreading along the H_u axis indicating the presence of weak local interaction field.

4. CONCLUSIONS

The PAN/PDLLA–Fe_3O_4 nanofibrous composite was obtained through electrospining setup with changed collector geometry. Fe_3O_4 magnetic nanoparticles are relative uniformly distributed throughout the composite PAN/PDLLA–Fe_3O_4 fibers nanoparticles as reflected from SEM images. Fibers diameters obtained from PAN/PDLLA decrease with the increase of the Fe_3O_4 nanoparticle concentration. The VSM measurements reveal the superparamagnetic behavior of PAN/PDLLA fibers containg Fe_3O_4 particles.

It is suggested that obtained PAN/PDLLA fibers–Fe_3O_4 nanoparticles (nanofibrous composites) could become a potential candidate for transportation systems and controlled release of drugs due to their strong magnetization.

Acknowledgements. S. Vulpe was supported by the Sectoral Operational Programme for Human Resources Development 2007–2013, co-financed by the European Social Fund, under the project number POSDRU/89/1.5/S/60746. Marin Adela and C. Necula were supported by the strategic grant POSDRU/89/1.5/S/58852, Project "Postdoctoral programme for training scientific researchers" cofinanced by the European Social Fund within the Sectorial Operational Program Human Resources Development 2007–2013. T.L. Mitran was supported by project number POSDRU/107/1.5/S/80765.

REFERENCES

1. T.M. Fahmy, P.M. Fong, A. Goyal, M. Saltzman, Mat. Today, **8**, *8*, 18–26 (2005).
2. V.P. Torchilin, Nat. Rev. Drug Discov., **4,** 145–160 (2005).
3. K. Egbaria, N. Weiner, Adv. Drug Deliv. Rev., **5**, 287-300 (1990).

4. R. Seema, C. Chanchal, S. Ravi, R. Ankur, K. Dinesh, S. Satish, D. Harish, Int. J. Drug Dev. & Res., **4**, *4*, 108–115 (2012).
5. H. Wei, R.X. Zhuo, X. Z. Zhang, Prog. Polym. Sci., **38**, *3–4*, 503–535 (2013).
6. N. Nishiyama, K. Kataoka, Pharmacol. Ther., **112**, *3*, 630–648 (2006).
7. U. Kedar, P. Phutane, S. Shidhaye, V. Kadam, Nanomed. Nanotech. Biol. Med., **6**, *6*, 714–729 (2010).
8. P. Saccardo, A. Villaverde, N. González-Montalbán, Biotechnol. Adv, **27**, *4*, 432–438 (2009).
9. P. K. Lo, K. L. Metera, H. F. Sleiman, Curr. Opin. Chem. Biol., **14**, *5*, 597–607 (2010).
10. Maria de la Fuente, M. Raviña, P. Paolicelli, A. Sanchez, B. Seijo, M. J. Alonso, Adv. Drug Deliv. Rev., **62**, *1*, 100–117 (2010).
11. A. Kumar, X. Zhang, X. J. Liang, Biotechnol. Adv., **31**, 593–606 (2013).
12. P. Blasi, S. Giovagnoli, A. Schoubben, M. Ricci, C. Rossi, Adv. Drug Deliv. Rev., **59**, *6*, 454–477 (2007).
13. S. Parveen, R. Misra, S. K. Sahoo, Nanomed. Nanotech. Biol. Med., **8**, *2*, 147–166 (2012).
14. S. Naahidi, M. Jafari, F. Edalat, K. Raymond, A. Khademhosseini, P. Chen, J. Control. Release, **166**, *2*, 182–194 (2013).
15. J. Dobson, Drug. Dev. Res., **67**, 55–60 (2006).
16. C. Suna, Jerry S.H. Leeb, M. Zhang, Adv. Drug Deliv. Rev., **60**, *11*, 1252–1265 (2008).
17. An-Hui Lu, E.L. Salabas, F. Schüth, Angew. Chem. Int. Ed. *46*, 1222–1244 (2007).
18. J. Klostergaard, Charles E. Seeney, Maturitas, **73**, *1*, 33–44 (2012).
19. Stuart C. McBain, Humphrey H.P., Yiu, J. Dobson, Int. J. Nanomedicine, **3**, *2*, 169–180 (2008).
20. Q. A. Pankhurst, J. Connolly, S.K. Jones, J. Dobson, J. Phys. D: Appl. Phys., **36**, R167-R181 (2003).
21. Q. Tian, C.D. Gomersall, A. Wong, P. Leung, G. Choi, G.M. Joynt, P. Tan, J. Lipman, Int. J. Antimicrob. Agents, **28**, 147–150 (2006).
22. U. Schwertmann, R. M. Cornell, *Iron oxides in the laboratory: Preparation and characterization*, Second Edition, Wiley-VCH, Weinheim, 2000.
23. R. J. Harrison, J. M. Feinberg, Geochem. Geophys. Geosyst., **9**, *5*, 05016, doi:10.1029/ 2008GC001987 (2008).
24. G. Aymeric, N. Herlin-Boime, C. Reynaud, C. Clinard, J.N. Rouzaud, Carbon, **40**, *15*, 2775–2789 (2002).
25. B. Dischler, A. Bubenzer, P. Koidi, Solid State Commn., **48**, *2*, 105–108 (1983).
26. D. Lin-Vien, N.B. Colthup, W.G. Fateley, J.G. Grasselli, *The Handbook of Infrared and Raman Characteristic Frequencies*, Academic Press, New York, 1991.
27. N.T. Paragkumar, E. Dellacherie, J.L. Six, Appl. Surf. Sci., **253**, 2758–2764 (2006).
28. T. Furukawa, H. Sato, R. Murakami, J. Zhang, I. Noda, Polymer, **48**, 1749–1755 (2007).
29. Carla M. B. Gonçalves, Joao A. P. Coutinho, Isabel M. Marrucho, *Poly (lactic acid): Synthesis, Structures, Properties, Processing, and Applications*, Chapter 8, Edited by R. Auras, L.T. Lim, Susan E. M. Selke, Hideto Tsuji, John Wiley & Sons, Inc., New Jersey, 2010.
30. D. Garlotta, J. Polym. Environ., **9**, *2*, 63–84 (2002).
31. N. Wang, Y. Guan, L. Yang, L. Jia, X. Wei, H. Liu, C. Guo, J. Colloid Interface Sci., **395**, 50–57 (2013).
32. C. Chen, X. Jiang, Y. V. Kaneti, A. Yu, Powder Technol., **236**, 157–163 (2013).
33. David J. Dunlop, J. Geophys. Res., **107**, *B3*, EPM 4-1–EPM 4-22 (2002).
34. A. P. Roberts, C. R. Pike, K. L. Verosub, J. Geophys. Res., **105**, *B12*, 28461–28475 (2000).
35. M. Hofmann-Amtenbrink, Brigitte von Rechenberg, H. Hofmann, *Nanostructured Materials for Biomedical Applications*, Chapter 5, Edited by M. C. Tan, Transworld Research Network, Kerala, India, 2009.
36. Lisa Tauxe, *Essentials of Paleomagnetism*, University of California Press, Berkeley, 2010.